



ELSEVIER

Available online at www.sciencedirect.com**ScienceDirect**journal homepage: www.elsevier.com/locate/he

Critical verification of the Kissinger theory to evaluate thermal desorption spectra

Andreas Drexler^{a,*}, Liese Vandewalle^b, Tom Depover^b, Kim Verbeken^b, Josef Domitner^a

^a Graz University of Technology, Institute of Materials Science, Joining and Forming, Research Group of Tools & Forming, Inffeldgasse 11/I, 8010, Graz, Austria

^b Ghent University, Department of Materials, Textiles and Chemical Engineering, Research Group Sustainable Materials Science, Technologiepark 46, 9052, Ghent, Belgium

HIGHLIGHTS

- Verification of the Kissinger theory and peak deconvolution procedure.
- Desorption energy fulfills the Kirchheim criterium based on bulk hydrogen diffusion.
- The R^2 -values do not necessarily mean trustworthy desorption energies.
- The TDS evaluation requires complete comprehension of the metal microstructure.

ARTICLE INFO

Article history:

Received 30 March 2021

Received in revised form

14 September 2021

Accepted 19 September 2021

Available online 11 October 2021

ABSTRACT

Multiple types of hydrogen trapping sites in advanced high-strength steels (AHSS) are often experimentally characterized by means of thermal desorption spectroscopy (TDS). The evaluation is regularly based on the peak deconvolution procedure combined with Kissinger's theory, which provides distinctive desorption energies of hydrogen trapping sites at microstructural defects. However, the desorption energies published in literature are often non-conclusive and from time to time contradictory in nature. Therefore, it is of utmost importance to verify the evaluation procedures according to Kissinger's theory for multiple types of hydrogen trapping sites. For that purpose, theoretical TDS spectra were simulated using a bulk diffusion model according to Oriani's theory. Binding energies and trap densities were chosen for providing TDS spectra with clearly separated as well as overlapping TDS peaks. Finally, the desorption energies according to Kissinger's theory were compared with the theoretical trapping energies used in the models. Based on this theoretical work, it is strongly recommended to apply the Kissinger theory only for the evaluation of single or well separated TDS peaks. If peaks overlap, complementary microstructural variation and characterization are a perquisite to correctly evaluate the TDS spectra.

© 2021 The Authors. Published by Elsevier Ltd on behalf of Hydrogen Energy Publications LLC. This is an open access article under the CC BY license (<http://creativecommons.org/licenses/by/4.0/>).

Keywords:

Hydrogen

Diffusion

Trapping

Thermal desorption spectroscopy

(TDS)

Modelling

Hydrogen embrittlement (HE)

* Corresponding author.

E-mail address: andreas.drexler@tugraz.at (A. Drexler).

<https://doi.org/10.1016/j.ijhydene.2021.09.171>

0360-3199/© 2021 The Authors. Published by Elsevier Ltd on behalf of Hydrogen Energy Publications LLC. This is an open access article under the CC BY license (<http://creativecommons.org/licenses/by/4.0/>).

Introduction

Hydrogen embrittlement (HE) is a crucial problem for advanced high-strength steels (AHSS), which may cause time-delayed brittle fracture of industrial components [1–6]. The delay in time is significantly influenced by hydrogen trapping at microstructural defects [7–11], which in turn affects.

- hydrogen uptake [12–15],
- chemical hydrogen diffusion [8,16,17],
- local accumulation at notches [4,18] or at punched edges [12] and
- the susceptibility to HE by reducing or increasing the diffusible hydrogen content [19–21].

Thermal desorption spectroscopy (TDS) is a suitable technique to investigate hydrogen trapping sites in the microstructure by measuring the hydrogen flux of a hydrogen charged sample during linear heating inside of a furnace [22–27]. Due to thermal activation, hydrogen is released from the trapping sites and diffuses out from the bulk sample [26,28–30]. Thus, the measured hydrogen flux profile against temperature allows to identify and quantify the sites of trapped hydrogen in the microstructure [28,29].

However, evaluating of the recorded TDS spectra is a difficult task and different experimental [31,32] and numerical evaluation methods [28,29,33–36] have been presented in literature. The most widely used experimental method is based on the Kissinger theory [31] and was introduced to hydrogen trapping by Choo and Lee [32]. It is based on a generalized thermodynamic concept originally derived to express the reaction rate of thermal dissociation of minerals. This experimental approach provides characteristic desorption energies for trapping sites at structural defects. The numerical evaluation of measured TDS spectra is a more generalized approach and allows to consider also the influence of sample geometry, hydrogen absorption during charging and hydrogen effusion during sample preparation on the TDS peak position and shape. For example, Polyanskiy et al. [37] studied the so-called skin-effect on measured TDS spectra and showed that an inhomogeneous hydrogen distribution before temperature ramping effects the desorption energies according to Kissinger.

The bulk diffusion model of Oriani [38] was already applied in several studies to numerically evaluate measured TDS spectra [28,29,33–35,39]. It assumes that the local relaxation between lattice sites and trapping sites is much faster than long-range chemical hydrogen diffusion [40]. This assumption is based on the experimental observation that hydrogen permeation through thin sheet metals containing trapping sites takes several minutes to hours [16], while permeation through well-annealed iron samples reaches stationary conditions after seconds [7,8,41]. Contrary to the often-cited division [2] of the Kissinger theory and the Oriani theory into “dissociation-controlled desorption” and “diffusion-controlled desorption”, respectively, Kirchheim [42] analytically derived the generalized Kissinger rate

equation by applying the bulk diffusion equation according to Oriani's theory. He also found a correlation between the desorption energy according to Kissinger and the activation energy of the chemical diffusion coefficient. In other words, it is likely that the retardation of chemical hydrogen diffusion out from bulky steel samples is based on the retrapping mechanism rather than on the thermal activation of de-trapping. Drexler et al. [29] performed a numerical validation of a parametrized bulk diffusion model according to Oriani, based on the experimental results of Depover et al. [26,30], by applying room temperature vacuum treatments before recording TDS spectra. During room temperature vacuum treatment shallow trapped hydrogen effused from the sample, while deep trapped hydrogen remained in the samples for much longer time. That resulted in a high temperature peak in the measured TDS spectra. Drexler et al. [4] also compared the experimental evaluation method according to the generalized Kissinger theory [42] with the numerical evaluation of measured TDS spectra according to Oriani. The TDS spectra consisted of a single peak and both evaluation methods were in very good agreement with respect to trapping energy and trap density.

However, while the original work of Kissinger [31] considered only a single type of trapping sites, the extension to multiple types of hydrogen trapping sites was done by TDS peak deconvolution in overlapping Gaussian curves [32]. A comprehensive verification of the Kissinger theory applied to the experimental evaluation of multiple types of hydrogen trapping sites with overlapping TDS peaks is still unexplored. Moreover, a comprehensive theory for explaining the peak deconvolution procedure with respect to hydrogen diffusion and trapping theories is missing. Therefore, the aim of the present study was the verification of the peak deconvolution procedure according to Kissinger with respect to a suitable bulk diffusion model according to Oriani. The model can.

- consider the influence of multiple types of trapping sites, of the sample size and of the heating rate,
- describe hydrogen outgassing during sample preparation and temperature ramping inside a furnace,
- evaluate the applicability of the Kissinger equation by Gaussian decomposition method of complex shaped TDS spectra and
- give new insights into the Kissinger theory with respect to bulk diffusion.

In the model, binding energies and trap densities were chosen to produce overlapping as well as clearly separated TDS peaks. The simulated TDS spectra were evaluated by applying the peak deconvolution method according to Kissinger's theory. Gaussian as well as asymmetric curves were used to determine the temperature at the peak maxima. The desorption energies according to Kissinger's theory were compared with the trapping energies used in the simulations. Differences between theoretical parameters and experimental parameters were critically discussed with respect to uniqueness of the peak deconvolution procedure and the site fraction of trapped hydrogen.

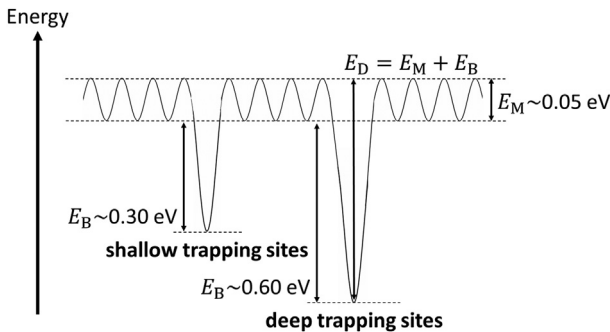


Fig. 1 – Schematic of hydrogen energy states considered in this work [43].

Theory

Basic equations for hydrogen bulk diffusion

The bulk diffusion-controlled model describing TDS has already been applied in several studies [4,8,28,29,33–35,42,44]. It splits the total hydrogen concentration into the interstitial lattice hydrogen concentration c_L and the trapped hydrogen concentrations $c_{T,i}$ at trapping site i [38] as

$$c = c_L + \sum_{i=1,N} c_{T,i} = c_L + c_T \quad (1)$$

where N is the total number of hydrogen trapping sites considered in the model and c_T is the total molar concentration of trapped hydrogen. Only the lattice hydrogen freely diffuses in the defect free lattice, while the trapped hydrogen occupies immobile and localized traps (as illustrated in Fig. 1). The hydrogen diffusion flux j according to Fick's first law must be reformulated concerning Eq. (1) and the multiple types of trapping sites at microstructural defects as

$$j = -D_L \text{grad}(c_L) = -D_L \frac{\partial c_L}{\partial c} \text{grad}(c) = -D_{\text{chem}} \text{grad}(c) \quad (2)$$

where D_L is the temperature dependent tracer diffusion coefficient of interstitial lattice hydrogen and D_{chem} is the concentration and temperature dependent chemical diffusion coefficient. The temperature dependence of the tracer diffusion coefficient D_L follows the Arrhenius function $D_{L,0} \exp(-E_M/RT)$, where E_M is the migration energy for lattice hydrogen, R is the universal gas constant and T is the temperature. The mass balance equation reflects the fact that the hydrogen diffusion flux j given in Eq. (2) equals the change of total hydrogen concentration in both lattice sites and trapping sites and this yields Fick's second law of hydrogen diffusion in steels as

$$\frac{dc}{dt} = \frac{dc_L}{dt} + \sum_{i=1,N} \frac{dc_{T,i}}{dt} = -\text{div}(j) = \text{div}(D_L \text{grad}(c_L)) \quad (3)$$

Note that Eq. (3) ignores the influences of macroscopic hydrostatic stress [12,45,46] and pipe diffusion along grain boundaries and dislocations as suggested by Toribio and Kharin [8,47,48] on the bulk diffusion in steels.

Oriani's theory

According to Oriani's local equilibrium theorem, the hydrogen exchange between interstitial lattice sites and trapping sites on nanoscale is much faster than the long range macroscopic diffusion [40]. This solid-state reaction can be expressed by the following reversible equation as



where H_T is the trapped hydrogen, V_L is the vacant lattice site, H_L is the interstitial lattice hydrogen and V_T is the vacant trapping site. In local equilibrium the trapped hydrogen concentration $c_{T,i}$ at the trapping site i can be expressed as a function of the site fraction of lattice hydrogen $y_L = c_L/N_L$ and the site fraction of trapped hydrogen $y_{T,i} = c_{T,i}/N_{T,i}$ as

$$\frac{y_L(1-y_{T,i})}{y_{T,i}(1-y_L)} = K_i = \exp\left(-\frac{E_{B,i}}{RT}\right) \quad (5)$$

N_L is the density of interstitial lattice sites, K_i is the equilibrium constant, $N_{T,i}$ is the trap density and $E_{B,i}$ is the corresponding binding energy for the trapping site i . Summing up all trap densities $N_{T,i}$ of N trapping sites gives the total trap density N_T as

$$N_T = \sum_{i=1,N} N_{T,i} \quad (6)$$

From a thermodynamic point of view, if two different microstructural defects have very similar binding energies $E_{B,i}$, their trap densities $N_{T,i}$ add to the same peak in the measured TDS spectra.

Using the mass balance Eq. (3) as a starting relation we can insert $y_{T,i}/N_{T,i}$ from Eq. (5) into $c_{T,i}$ on the left side. Keeping in mind that recording TDS spectra with a defined heating rate θ causes both $c_{T,i}(t)$ and $T(t)$ being time dependent and thus

$$\frac{dc_{T,i}}{dt} = \frac{\partial c_{T,i}}{\partial c_L} \frac{dc_L}{dt} + \frac{\partial c_{T,i}}{\partial T} \theta \quad (7)$$

Inserting Eq. (7) into the mass balance Eq. (3) yields the governing partial differential equation (PDE) for lattice hydrogen diffusion in steels [49] with sink and source terms for multiple hydrogen trapping sites with local equilibrium as following

$$\frac{dc_L}{dt} \left(1 + \sum_{i=1,N} \frac{N_{T,i} K_i}{N_L (K_i + c_L (1 - K_i)/N_L)^2} \right) - \sum_{i=1,N} \frac{c_L N_{T,i} K_i (1 - c_L/N_L)}{N_L (K_i + c_L (1 - K_i)/N_L)^2} \frac{E_{B,i}}{RT^2} \exp\left(-\frac{E_{B,i}}{RT}\right) \theta = D_L \text{grad}(c_L) \quad (8)$$

Kissinger's theory

In the work of Choo and Lee [32], the thermal excitation of trapped hydrogen to interstitial lattice sites is assumed to be expressed as



which is a simplification of the more generalized Eq. (4), proposing that the number of vacant interstitial lattice sites is numerous and stays unchanged by de-trapping. To describe the hydrogen escape rate from hydrogen trapping site i , Choo and Lee suggested the use of the Kissinger theory [31] as

$$\frac{dx_i}{dt} = A(1 - x_i)^n \exp\left(-\frac{E_{D,i}}{RT}\right) \quad (10)$$

where $x = 1 - c_{T,i}/c_{T,i,t=0}$, $c_{T,i,t=0}$ is the initial trapped hydrogen concentration, A is a constant pre-factor, R is the universal gas constant and T is the temperature. This well-known rate equation can easily be simplified to

$$\frac{dc_{T,i}}{dt} = -Ac_{T,i}^n \exp\left(-\frac{E_{D,i}}{RT}\right) \quad (11)$$

which is very similar to the backward reaction term in the trapping equation published previously by Drexler et al. [29]. According to irreversible thermodynamics [42], the desorption energy $E_{D,i}$ depends on the rate-determining processes in the microstructure and can be.

- the activation energy for bulk diffusion,
- the desorption energy of adsorbed hydrogen at the surface,
- the de-trapping energy of trapped hydrogen or
- the decomposition energy of a compound releasing species.

According to chemical kinetics, the exponent n is unity for gaseous hydrogen release by thermal desorption from a steel sample [50]. At the maximum release rate of Eq. (11), the well-known Kissinger equation is obtained as

$$\ln\left(\frac{\theta}{T_m^2}\right) = -\frac{E_{D,i}}{RT_m} + \ln(Y) \quad (12)$$

where T_m is the temperature at the peak maximum. Kirchheim [42] generalized the Kissinger theory with respect to hydrogen trapping, considering the influence of sample geometry and trap density $N_{T,i}$ on the TDS peak position and size. Therefore, the intercept $\ln(Y)$ with the y-axis in the Choo-Lee plot fulfills the following relationship in case of bulk diffusion-controlled thermal desorption [42]:

$$Y \sim \frac{c_L}{s^2 N_{T,i} E_{D,i}} \quad (13)$$

where s is the sample thickness.

Methodological approach

Numerical modelling and parametrization

The PDE given in Eq. (8) for multiple types of hydrogen trapping sites was numerically solved in one-dimensional form by using the finite difference method (FDM) [51], which was programmed in python. A uniform mesh with equidistant nodes with a distance of 1 μm were arranged through the thickness of the specimen. The element size was sufficient to obtain mesh independent results. A time step of 1 s leaded to converged simulation results. To describe hydrogen effusion from the surface of the sample during temperature ramping, the Dirichlet boundary condition was applied as

$$c_L\left(\pm\frac{s}{2}, t\right) = 0 \quad (14)$$

where t is the time. The trap density $N_{T,i}$ and the initial lattice hydrogen concentration $c_{L,0}$ were homogenously distributed in the sample. Due to the zero conditions at the boundary, as given in Eq. (14), and the uniform initial hydrogen concentration in the inner part, the hydrogen concentration gradient at the boundary leads to very high values of the hydrogen flux at the beginning of the simulation. A decreasing flux at the beginning of measured TDS spectra can also be observed in some publications, when the time for sample handling between charging and measurement is sufficiently small [30,52]. To work around this problem, fluxes were only shown above a sample temperature of 40 °C.

Furthermore, a spatially uniform temperature field $T(t)$ was assumed in the model. The temperature T is defined at any time by a constant heating rate θ as following

$$T(t) = T_0 + \theta t \quad (15)$$

where T_0 is the initial temperature being 21 °C. Inhomogeneous, temperature fields may arise, when recording TDS spectra of thick samples and at high heating rates compared to thermal diffusion [53,54]. Nevertheless, the effect of inhomogenous temperature fields was not considered in the present work and will be thoroughly investigated in our future studies. In addition, no skin-effects were taken into account in the present work [12,37,55]. The parameters of the bulk diffusion model were subdivided into two sets:

- while set A contained all parameters, which were constant throughout the present study and were taken from literature,
- set B contained the number of trapping sites N , binding energies $E_{B,i}$, trap densities $N_{T,i}$ and initial lattice hydrogen concentrations $c_{L,0}$.

Parameters of set A are given in Table 1. In accordance to Svoboda and Fischer [56], a volume of 4900 mm^3 was chosen for

Table 1 – Set A of the bulk diffusion parameters.

Parameter	Value	Reference
Density of interstitial lattice sites N_L	$2.041 \cdot 10^{-4} \text{ mol/mm}^3$	[56]
Jump frequency $D_{L,0}$	$0.133 \text{ mm}^2/\text{s}$	[60–62]
Migration energy E_M	5.63 kJ/mol	[60–62]
Sample thickness s	1 mm	

Table 2 – Set B of the bulk diffusion parameters.

Model No.	Number of traps N	Trapping site number i	Binding energy $E_{B,i}$ [kJ/mol]	Trap density $N_{T,i}$ [mol/mm ³]	Initial lattice hydrogen concentration $c_{L,0}$ [mol/mm ³]	Total hydrogen content \bar{c} [wppm]
1	1	1	30	10^{-7}	10^{-15}	10^{-5}
2					10^{-10}	1.26
3					10^{-9}	6.77
4	1	1	50	10^{-7}	10^{-15}	0.05
5					10^{-10}	12.74
6					10^{-9}	12.88
7	1	1	70	10^{-7}	10^{-15}	11.94
8					10^{-10}	12.77
9					10^{-9}	12.89
10	2	1	30	10^{-7}	10^{-10}	2.54
		2	70	10^{-8}		
11	2	1	30	10^{-7}	10^{-10}	2.54
		2	50	10^{-8}		
12	3	1	30	10^{-7}	10^{-10}	2.54
		2	50	$5 \cdot 10^{-9}$		
		3	70	$5 \cdot 10^{-9}$		

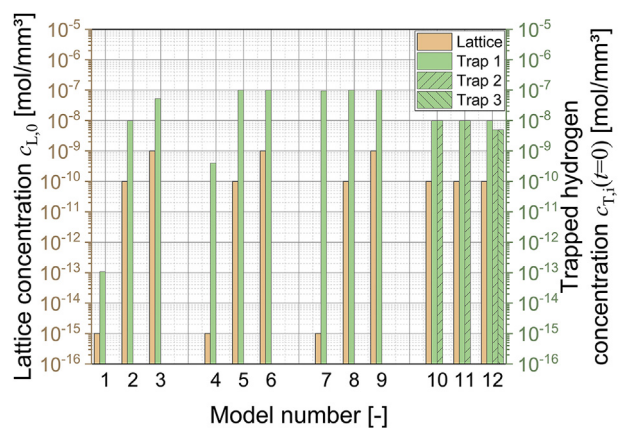
1 mol of tetrahedral lattice sites [57–59] in the samples, resulting in a density of interstitial lattice sites N_L of $2.041 \cdot 10^{-4}$ mol/mm³. The migration energy E_M of 5.63 kJ/mol and the jump frequency $D_{L,0}$ of 0.133 mm²/s were averaged over different literature sources [60–62]. The sample thickness s was 1 mm and is in the range of typical AHSS sheet thicknesses [3,4,63].

The parameters of set B, as summarized in Table 2, were varied to study their influence on the TDS peak evaluation, applying the peak deconvolution method according to the Kissinger theory. The investigated binding energies $E_{B,i}$ were 30 kJ/mol, 50 kJ/mol and 70 kJ/mol and can be motivated as follows:

- 30 kJ/mol corresponds for example to hydrogen trapping sites at dislocations or at martensitic lath boundaries [8,9,64] in dual phase AHSS [4,65].
- 50 kJ/mol is a binding energy $E_{B,i}$ slightly below the often cited threshold for “quasi-irreversible” hydrogen trapping sites [66] and presents trapping sites e.g. at carbide interfaces in a martensitic matrix [28,67].
- 70 kJ/mol is the binding energy $E_{B,i}$ of very deep trapping sites and could be introduced into the microstructure during thermal processing [29] or during severe plastic deformation [8,12]. These trapping sites stay filled with hydrogen even after long lasting vacuum treatments at room temperature before TDS [28,64].

The corresponding equilibrium constants K_i at room temperature determining the site fractions $y_{T,i}$ of trapped hydrogen are $4.5 \cdot 10^{-6}$, $1.23 \cdot 10^{-9}$ and $3.36 \cdot 10^{-13}$, respectively. A trap density $N_{T,1}$ of 10^{-7} mol/mm³, as chosen for trap 1, is representative for a dislocation density of around 10^{14} m/m³ [8]. Trap densities of trap 2 $N_{T,2}$ and trap 3 $N_{T,3}$ were 10^{-8} mol/mm³ or $5 \cdot 10^{-9}$ mol/mm³. These values were found by Drexler et al. [28,29] to represent deeper trapping sites, e.g. at carbide interfaces.

While initial lattice hydrogen concentrations $c_{L,0}$ between 10^{-15} mol/mm³ to 10^{-10} mol/mm³ represent hydrogen uptake

**Fig. 2 – Initial concentrations of hydrogen in the lattice sites and trapping sites.**

from corrosive or electrochemical sources [4,68], the initial lattice hydrogen concentration $c_{L,0}$ of 10^{-9} mol/mm³ represents full occupation of trapping sites and thus, hydrogen accommodation at the interstitial lattice sites. Fig. 2 shows the initial concentration of hydrogen in the lattice and trapping sites graphically. The corresponding total hydrogen contents \bar{c} are given in Table 2 and are calculated from the molar total hydrogen concentration c as following

$$\bar{c} = \frac{c \cdot 10^6 \cdot M_H}{\varrho} \quad (16)$$

where M_H is the molar mass of hydrogen and ϱ is the density of the sample. The hydrogen content increases with both increasing binding energy $E_{B,i}$ and increasing initial lattice hydrogen concentration $c_{L,0}$. Basically, the initial lattice hydrogen concentration $c_{L,0}$ is in good agreement with the lattice hydrogen concentration c_L found for electrochemical hydrogen charged materials [4,8,63].

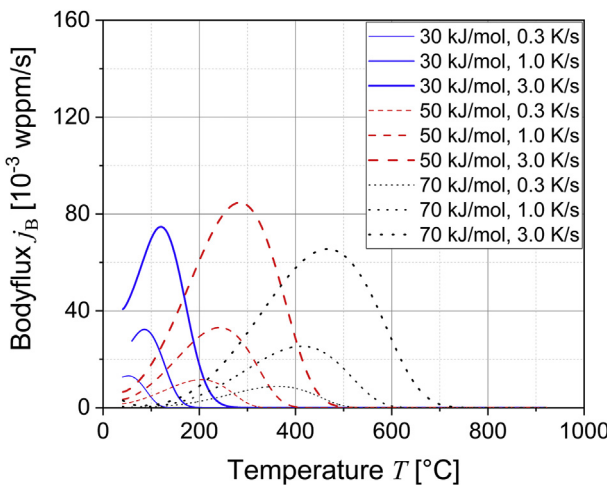


Fig. 3 – Simulated TDS spectra for a single type of hydrogen trapping sites.

Experimental evaluation of TDS spectra

To evaluate the measured TDS spectra with respect to the Kissinger theory, the temperature of the peak maxima T_m must be determined as a function of the heating rate θ . In case of single peaks, this was rather straightforward using the temperature T_m at the TDS peak maximum. In case of multiple types of hydrogen trapping sites, a distinction was made between hydrogen trapping causing

- clearly separated peaks and
- overlapping peaks.

For clearly separated peaks, the temperature at the peak maxima T_m was again determined straightforward. However, this was not possible for overlapping peaks. Therefore, for different types of hydrogen trapping site i the temperatures of the peak maxima $T_{m,i}$ were identified and analysed individually by a peak deconvolution method, fitting a sum of Gaussian and/or asymmetric peaks to the simulated TDS

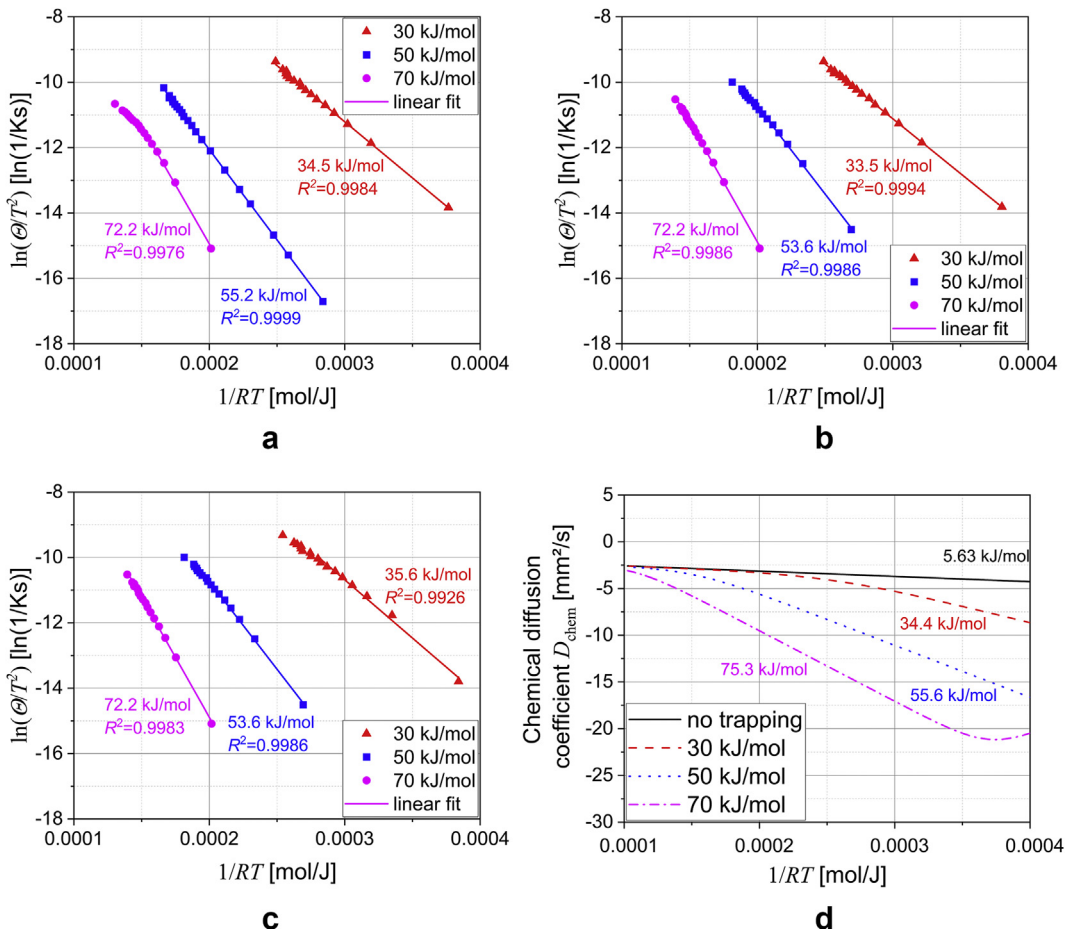


Fig. 4 – Choo-Lee plots for a single type of trapping sites with initial lattice hydrogen concentrations $c_{L,0}$ of a) $10^{-15} \text{ mol/mm}^3$, b) $10^{-10} \text{ mol/mm}^3$ and c) 10^{-9} mol/mm^3 . d) Arrhenius plot of the tracer diffusion coefficient D_L and the corresponding chemical diffusion coefficients D_{chem} .

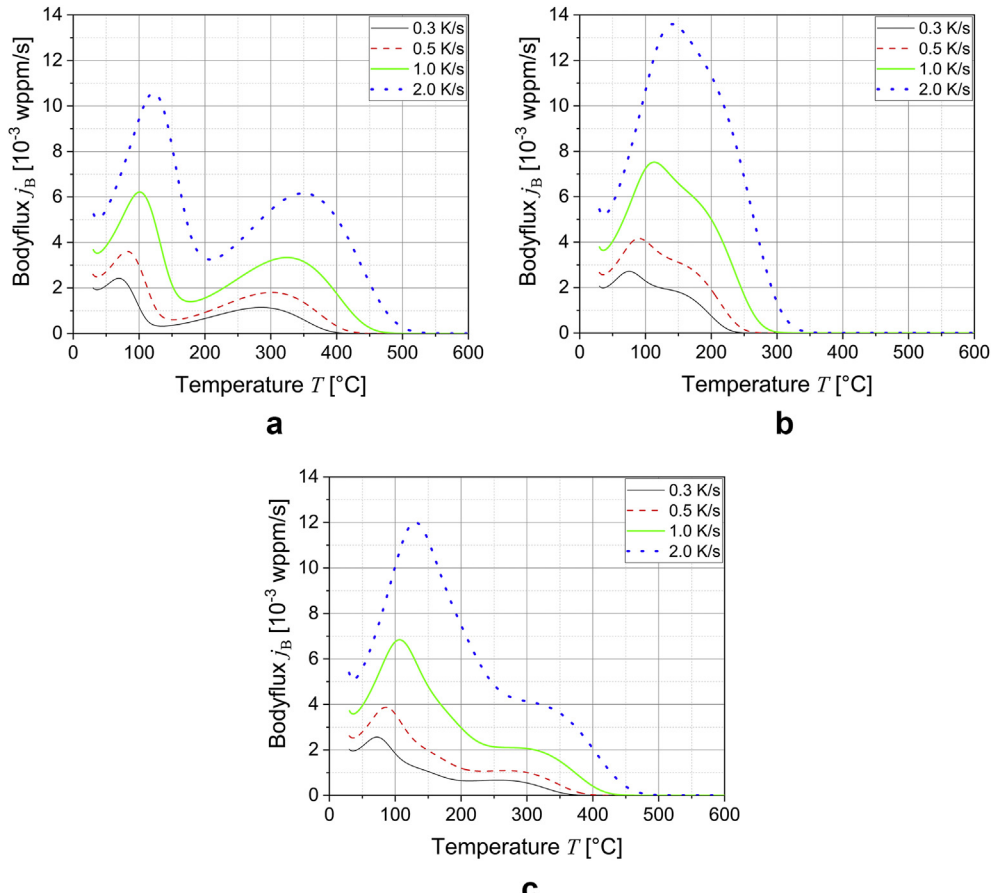


Fig. 5 – Simulated TDS spectra considering multiple hydrogen trapping sites with binding energies $E_{B,i}$ of a) 30 kJ/mol and 70 kJ/mol, b) 30 kJ/mol and 50 kJ/mol and c) 30 kJ/mol, 50 kJ/mol and 70 kJ/mol.

spectra. These fitted curves were then independently evaluated according the Kissinger theory. The equations and fitting parameters of the Gaussian and asymmetric peaks are summarized in the Appendix.

Results and discussion

General aspects of bulk diffusion

According to Oriani's theory, the shift of the peak of the body-flux j_B to higher temperatures by increasing the heating rate θ , trap density $N_{T,i}$ or binding energy $E_{B,i}$ is related to the bulk diffusion of hydrogen to the surface. The actual chemical diffusion coefficient D_{chem} , as defined in Eq. (2), ranges over several orders of magnitude depending on the local concentration and temperature [26,29]. For example, in a steel containing a sufficiently high density of carbides the effective diffusion coefficient D_{eff} [30] at room temperature can be orders of magnitude lower than the tracer diffusion coefficient D_L in

pure iron [7,8,60]. In other words, a higher trap density N_T retards hydrogen diffusion to the surface, which shifts the recorded TDS peak to higher temperatures. The effect of binding energy $E_{B,i}$ on the peak position becomes obvious as according to Eq. (4) and Eq. (5) around 99% of the total hydrogen is trapped in the sample at room temperature [4]. By increasing the temperature, thermal activation of the trapping sites leads to an increase of both the lattice hydrogen concentration c_L and the chemical diffusion coefficient D_{chem} . As the chemical diffusion coefficient depends also on the local hydrogen concentration, which is contradictory to the often cited concept of effective diffusion coefficient D_{eff} [16,17], diffusion occurs in the region of high hydrogen concentrations faster than regions with low hydrogen concentrations. In other words, in regions of low concentrations hydrogen re-trapping is more intense and retards bulk diffusion of hydrogen to the surface. This extreme asymmetry in the chemical diffusion between inner and outer regions of the TDS sample, contributes to the shape and position of the recorded TDS peaks and makes a numerical evaluation necessary.

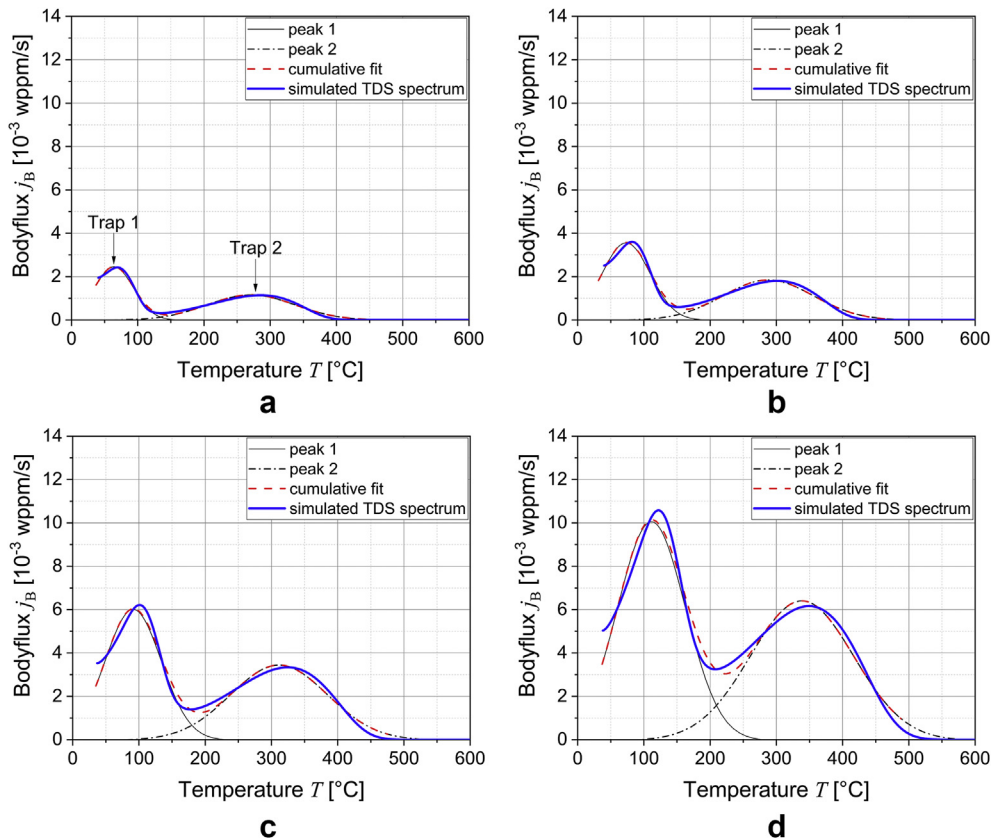


Fig. 6 – Simulated TDS spectra considering two types of trapping sites with binding energies $E_{B,i}$ of 30 kJ/mol and 70 kJ/mol. Peak deconvolution procedure using Gaussian curves for heating rates θ of a) 0.3 °C/s, b) 0.5 °C/s, c) 1 °C/s and d) 2 °C/s.

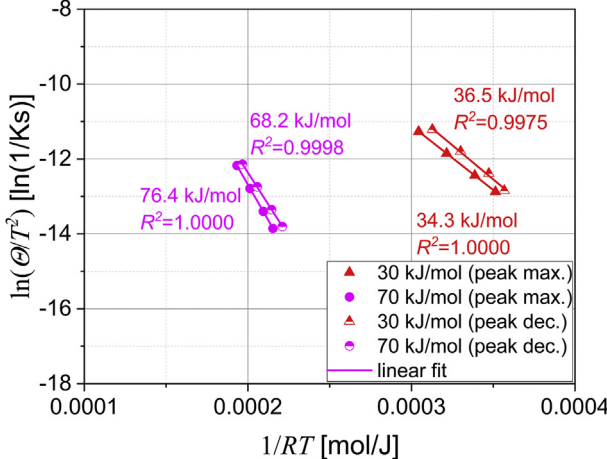


Fig. 7 – Choo-Lee plot of the simulated TDS spectra considering two types of trapping sites with binding energies $E_{B,i}$ of 30 kJ/mol and 70 kJ/mol. The temperatures of the peak maxima were evaluated straightforward by the temperature of the TDS peak maxima and by applying the peak deconvolution procedure using Gaussian curves.

Single type of hydrogen trapping sites

As shown in Fig. 3, TDS spectra were simulated for materials containing a single type of hydrogen trapping sites for different binding energies $E_{B,i}$ and an initial lattice hydrogen concentration $c_{L,0}$ of 10^{-9} mol/mm³. The total hydrogen contents were between 6.77 wppm to 12.89 wppm depending on the binding energy $E_{B,i}$. During heating of the samples with constant heating rate θ the tracer hydrogen diffusion coefficient D_L increases and the equilibrium constant K_i becomes unity. Hydrogen trapping sites are fully activated at high temperatures and do not effectively bind hydrogen. Especially, shallow hydrogen trapping sites do not contribute to the chemical diffusion coefficient D_{chem} at high temperatures. The same effect occurs at room temperature, when all hydrogen trapping sites are fully occupied by hydrogen and a further increase of the total hydrogen concentration c can only be accommodated by the interstitial lattice sites.

The simulated TDS spectra were evaluated according to Kissinger's theory using the temperature of the peak maxima. The heating rates θ were increased from 0.1 °C/s to 20 °C/s. The corresponding Choo-Lee plots are given in Fig. 4a, b and c for three different initial lattice hydrogen concentrations $c_{L,0}$ of 10^{-15} mol/mm³, 10^{-10} mol/mm³ and 10^{-9} mol/mm³, respectively. The R^2 -values for the linear fits are approximately unity

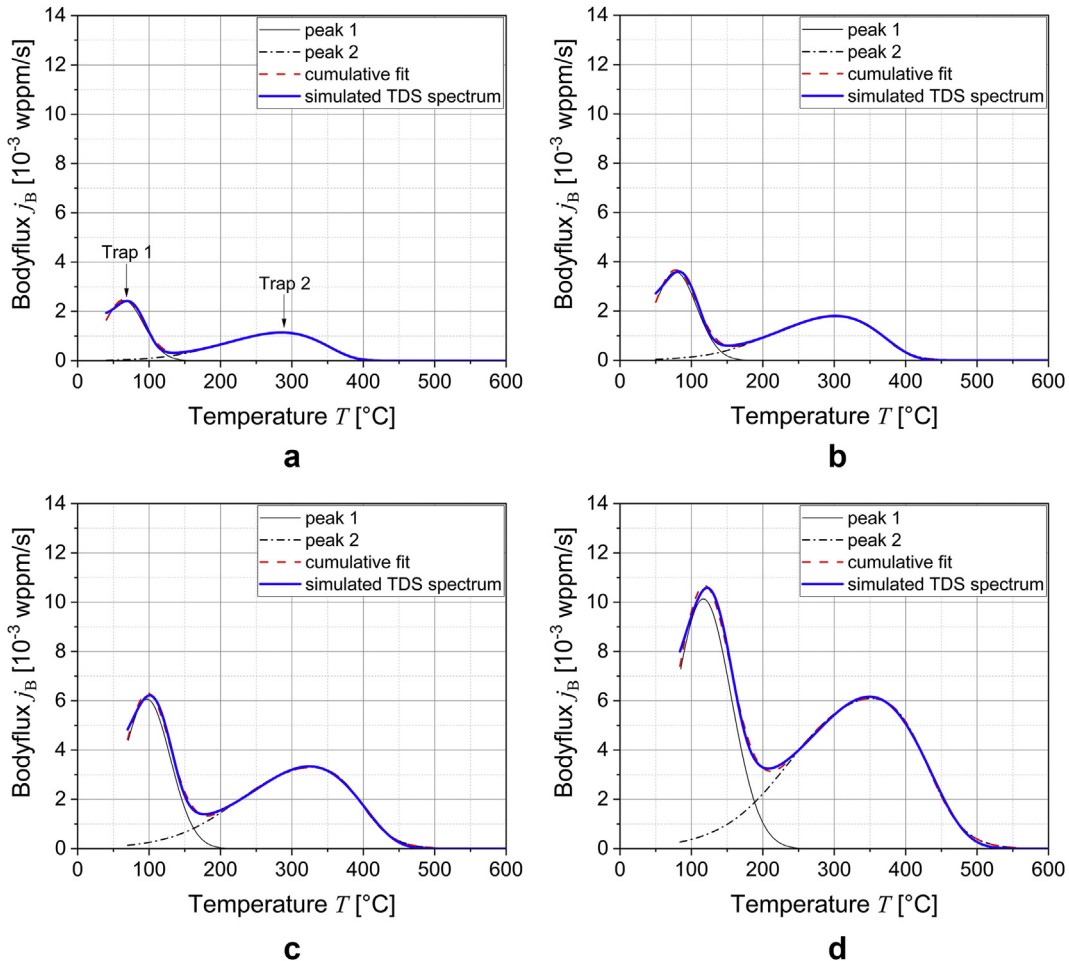


Fig. 8 – Simulated TDS spectra considering two types of trapping sites with binding energies $E_{B,i}$ of 30 kJ/mol and 70 kJ/mol. Peak deconvolution procedure using a mixture of Gaussian and asymmetric curves for heating rates θ of a) 0.3 °C/s, b) 0.5 °C/s, c) 1 °C/s and d) 2 °C/s.

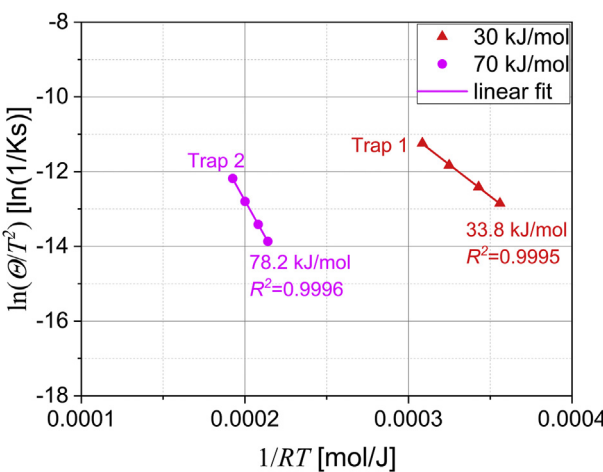


Fig. 9 – Choo-Lee plot of the simulated TDS spectra considering two types of trapping sites with binding energies $E_{B,i}$ of 30 kJ/mol and 70 kJ/mol. The temperatures of the peak maxima were evaluated by applying the peak deconvolution procedure using an asymmetrical curve for the higher temperature TDS peak of trap 2.

in the Choo-Lee plots, which represents almost perfect linearity. The slopes in the linear regimes represent $E_{D,i}$, which is always higher than the binding energies $E_{B,i}$ and which can be approximated by the Kirchheim criterion [42] as

$$E_{D,i} \equiv E_{B,i} + E_M. \quad (17)$$

A slight curvature can be observed in Fig. 4a, b and c at lower desorption energies $E_{D,i}$ with increasing temperatures and heating rates θ . This is most pronounced at low hydrogen concentrations c and high binding energies $E_{B,i}$.

To the authors knowledge, Kirchheim [42] was first who showed that Oriani's theory of local equilibrium [38] yields straight lines in the Choo-Lee plot. However, different hydrogen trapping approaches for steels are still debated at conferences and in literature [69]. For example, Nagumo separated in his famous book [2] "Fundamentals of Hydrogen Embrittlement" Kissinger's theory from the local equilibrium approach and argued that straight lines are related to dissociation-controlled desorption. Due to the ongoing discussion, we would like to emphasize the correlation between experimental observations and the predictions of the theoretical trapping theories.

$$D_{\text{chem}} = \frac{D_L}{2} \left(1 + \left(\frac{c(1-K)}{N_L} - \frac{N_T}{N_L} + K \right) \cdot \sqrt{\left(\frac{c(1-K)}{N_L} - K - \frac{N_T}{N_L} \right)^2 + \frac{4cK(1-K)}{N_L}} \right) \quad (18)$$

For the interpretation of the evaluated desorption energy $E_{D,i}$ according to Kissinger, the chemical diffusion coefficient D_{chem} was calculated [56] as

The corresponding Arrhenius plot is given in Fig. 4d. It is obvious that the chemical diffusion coefficients D_{chem} cannot be described by a simple Arrhenius function, because of its complex concentration and temperature dependency [56]. Comparing the evaluated desorption energies $E_{D,i}$ according Kissinger's theory with the activation energies for bulk diffusion in the linear regimes shows good agreement. The positive curvature in the Choo-Lee plot corresponds with the positive curvature in the Arrhenius plot of the chemical diffusion coefficients D_{chem} and is attributed to the thermal activation of hydrogen trapping sites. A similar tendency was observed by Rhode et al. [53], measuring TDS spectra of T24 welds. Due to thermal activation, less hydrogen is effectively trapped at elevated temperatures and interstitial lattice hydrogen diffusion becomes the rate limiting mechanism in the bulk diffusion model. In other words, the chemical diffusion coefficient D_{chem} increases with temperature and

its maximum corresponds to the lattice hydrogen diffusion coefficient D_L .

Multiple types of hydrogen trapping sites

Three different TDS spectra were simulated considering multiple types of trapping sites. The corresponding binding energies $E_{B,i}$ and trap densities $N_{T,i}$ are given in Table 2. The corresponding TDS spectra depending on four different heating rates θ are shown in Fig. 5. Only when the binding energies $E_{B,i}$ were very different, i.e., at 30 kJ/mol and 70 kJ/mol, two clearly separate peaks can be observed in the TDS spectra, as shown in Fig. 5a. However, when the binding energies $E_{B,i}$ were too close, overlapping of the peaks occurred, as shown in Fig. 5b and c.

TDS spectra with clearly separate peaks

Fig. 6 shows the simulated TDS spectra using binding energies $E_{B,i}$ of 30 kJ/mol and 70 kJ/mol. They consist of two more or less separate TDS peaks. In this case, the TDS peaks

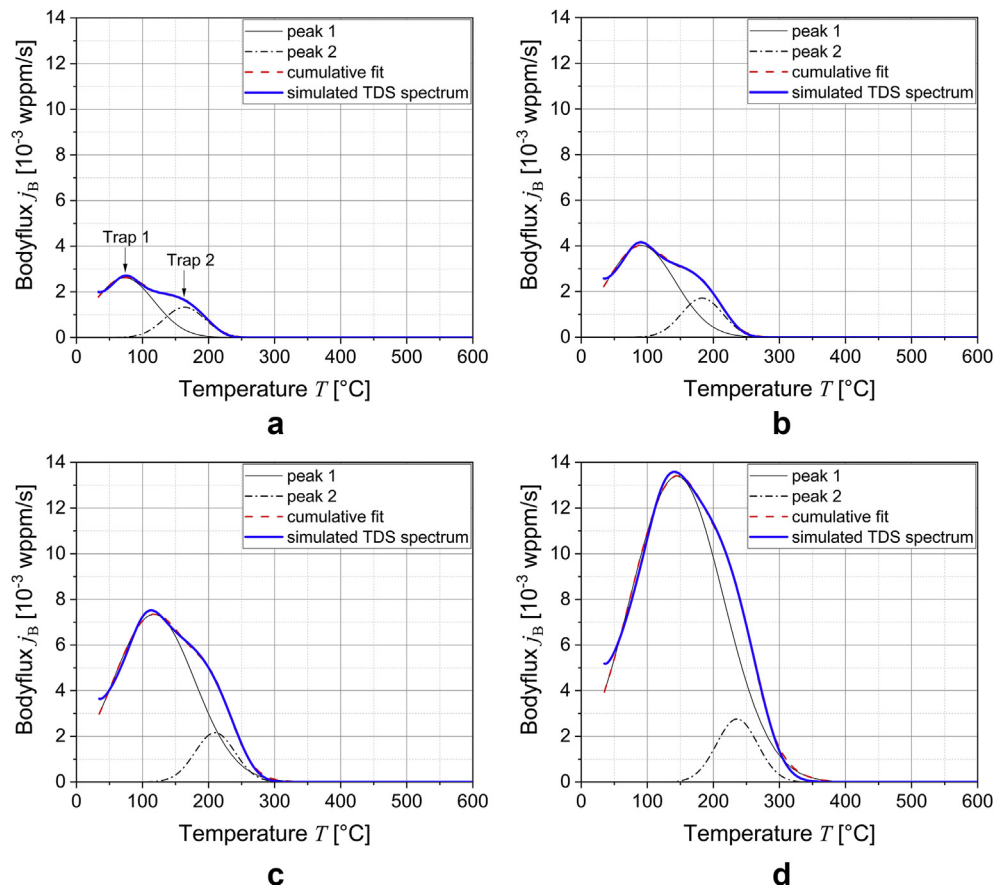


Fig. 10 – Simulated TDS spectra considering two types of trapping sites with binding energies $E_{B,i}$ of 30 kJ/mol and 50 kJ/mol. Peak deconvolution procedure using Gaussian curves for heating rates θ of a) 0.3 °C/s, b) 0.5 °C/s, c) 1 °C/s and d) 2 °C/s.

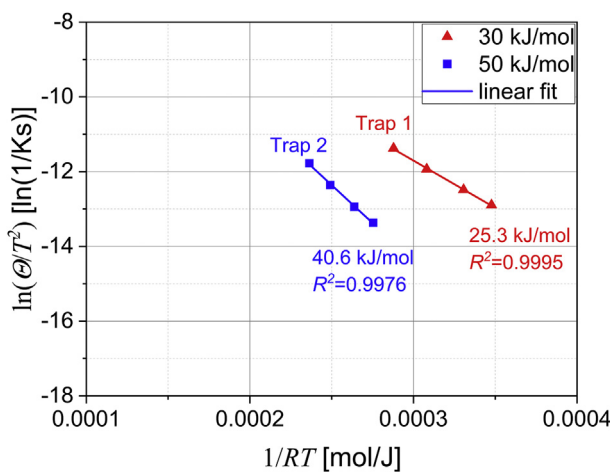


Fig. 11 – Choo-Lee plot of the simulated TDS spectra considering two types of trapping sites with binding energies $E_{B,i}$ of 30 kJ/mol and 50 kJ/mol. The temperatures of the peak maxima were evaluated by applying the peak deconvolution procedure using Gaussian curves.

were analysed according to the Kissinger theory both on their peak maximum as well as by fitting Gaussian peaks to the TDS spectrum. The TDS peak deconvolution into two Gaussian peaks is shown in Fig. 6 and the corresponding Choo-Lee plot is shown in Fig. 7. By using the temperature of

the peak maxima, desorption energies $E_{D,i}$ of 34.3 kJ/mol and 76.4 kJ/mol were obtained for the evaluation of the first and the second peak, respectively. Consequently, also for the presence of two peaks the bulk diffusion approach fulfils the Kirchheim criterion given in Eq. (17). However, when the method of Gaussian peak fitting was used, desorption energies $E_{D,i}$ of 36.5 kJ/mol and 68.2 kJ/mol were obtained. Hence, the use of the Kissinger theory in combination with Gaussian peak fitting resulted in an underestimation of the corresponding desorption energy $E_{D,2}$ of trap 2. Furthermore, it can also be seen from Fig. 6 that the shape of the TDS peaks deviates from the shape of the Gaussian curve and hence fitting of the Gaussian peaks to this spectrum leads to relatively poor agreement of the peak maxima.

A second type of fitting was performed, where the TDS peak of trap 2 was fitted using the asymmetric function while the TDS peak of trap 1 was Gaussian. This resulted in better agreement between the fitted spectrum and the simulated spectrum, as shown in Fig. 8. Moreover, better correspondence of the desorption energies $E_{D,i}$ to the Kirchheim criterium, as shown in Fig. 9, was obtained. However, it must be noted that the best agreement is still obtained by using the peak maxima of the simulated spectra.

TDS spectra with overlapping peaks

As shown in Fig. 10, the simulated TDS spectra for binding energies $E_{B,i}$ of 30 kJ/mol and 50 kJ/mol consist out of a peak with a “shoulder” at the high temperature rather than two

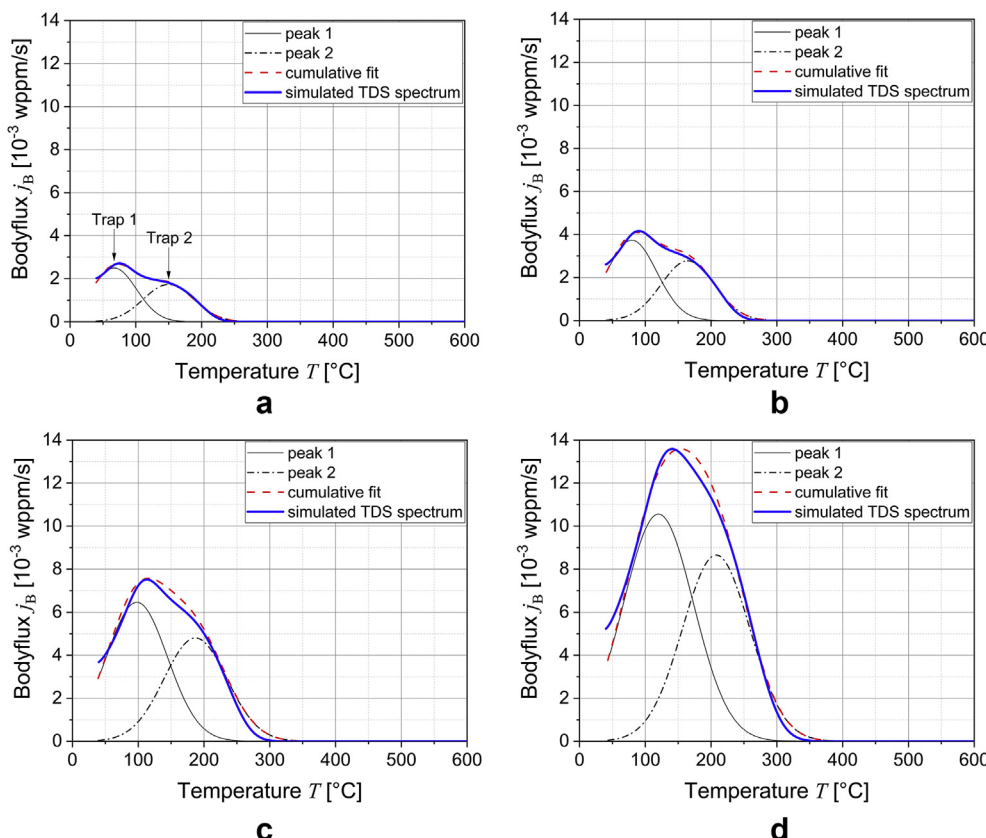


Fig. 12 – Simulated TDS spectra considering two types of trapping sites with binding energies $E_{B,i}$ of 30 kJ/mol and 50 kJ/mol “Improved” peak deconvolution procedure using Gaussian curves for heating rates θ of a) 0.3 $^\circ\text{C/s}$, b) 0.5 $^\circ\text{C/s}$, c) 1 $^\circ\text{C/s}$ and d) 2 $^\circ\text{C/s}$.

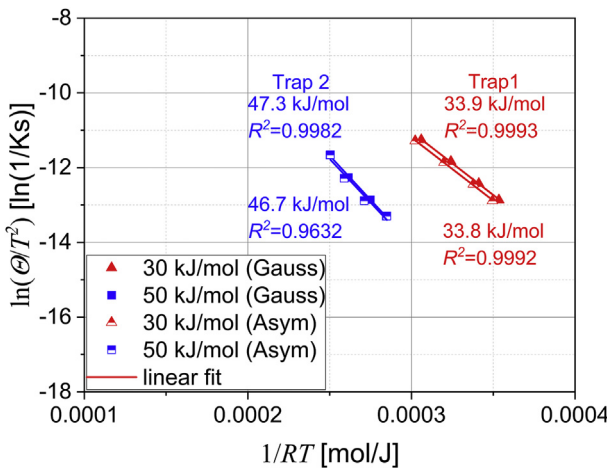


Fig. 13 – Choo-Lee plot of the simulated TDS spectra considering two types of trapping sites with binding energies E_B of 30 kJ/mol and 50 kJ/mol. The temperatures of the peak maxima were evaluated by applying the “improved” peak deconvolution procedure using Gaussian curves as well as fitting using an assymetrical curve for trap 2.

separate peaks. When simply fitting the Gaussian curves, the Kissinger equation resulted in desorption energies $E_{D,i}$ of 25.3 kJ/mol and 40.6 kJ/mol for the evaluation of trap 1 and

trap 2, respectively. This is significantly lower than the binding energies $E_{B,i}$ of the trapping sites, and hence no agreement was obtained between the Kissinger approach and the bulk diffusion approach. However, as illustrated in Fig. 11, the R^2 -values of the linear fits were approximately unity, i.e. 0.9995 for trap 1 and 0.9976 for trap 2. Consequently, a good R^2 -value, which is often used as verification method, does not necessarily confirm that the results are reliable.

According to the Choo-Lee method, the area under a desorption peak should represent the amount of hydrogen trapped at the corresponding trapping site. Therefore, the peak area should scale with the amount of trapped hydrogen at the trapping sites and the heating rate θ . When looking at the Gaussian peak deconvolution method in more detail, it can be seen in Fig. 10 that the Gaussian peaks corresponding to trap 2 do not scale with the different heating rates θ , but remain at a similar height independently of the applied heating rate θ . Furthermore, the peak area of trap 2 is often significantly smaller than of trap 1. The peak area should scale with the amount of trapped hydrogen at the trapping sites and the heating rate θ . According to Eq. (5) and the corresponding trapping parameters in Table 2, equal amounts of hydrogen should be present in trap 1 and trap 2. This equal ratio of trapped hydrogen is in contradiction to the first Gaussian peak deconvolution with a smaller peak area for trap 2 than for trap 1. Consequently, more care should be taken when fitting Gaussian peaks to the spectrum.

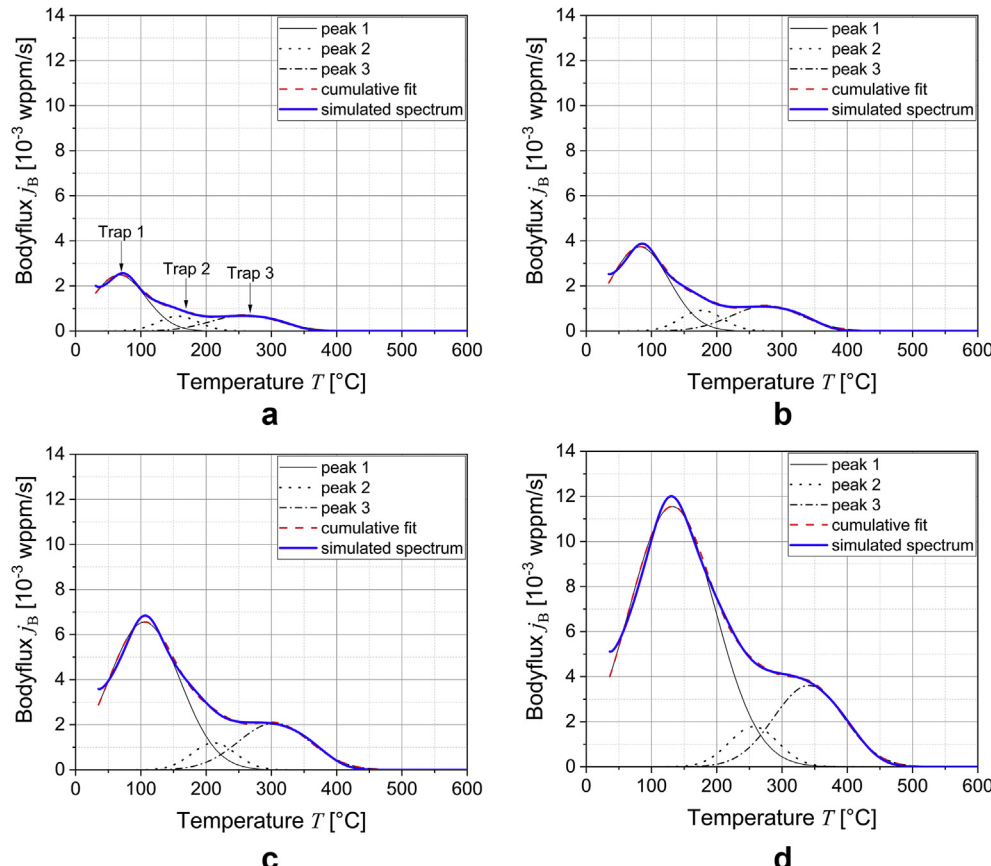


Fig. 14 – Simulated TDS spectra considering three types of trapping sites with binding energies $E_{B,i}$ of 30 kJ/mol, 50 kJ/mol and 70 kJ/mol. Peak deconvolution procedure using Gaussian curves for heating rates θ of a) 0.3 °C/s, b) 0.5 °C/s, c) 1 °C/s and d) 2 °C/s.

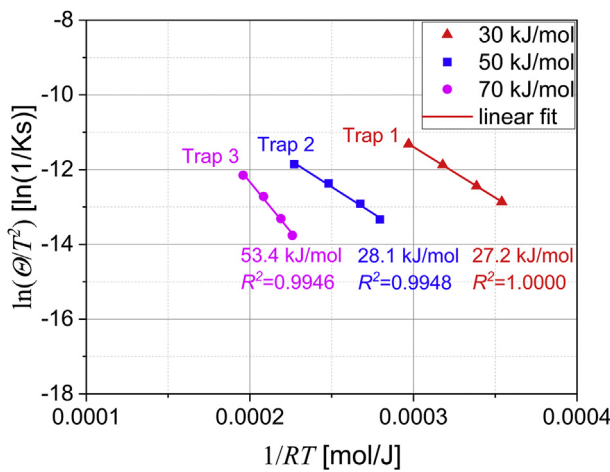


Fig. 15 – Choo-Lee plot of the simulated TDS spectra considering three types of trapping sites with binding energies $E_{B,i}$ of 30 kJ/mol, 50 kJ/mol and 70 kJ/mol. The temperatures of the peak maxima were evaluated by applying the peak deconvolution procedure using Gaussian curves.

This was done in a second fitting procedure where restrictions were imposed related to the peak areas, as shown in Fig. 12. Since a similar hydrogen concentration at trap 1 and trap 2 was present, the parameters B_1 and B_2 , describing the area under the peaks should be the same as well and should equal $B_{\text{tot}}/2$, with B_{tot} the area corresponding to total amount of trapped hydrogen. However, to allow some variation, the range over which B_1 and B_2 should be optimized incorporated a 5% deviation from $B_{\text{tot}}/2$. The evaluation of the desorption energy $E_{D,i}$ according to the Kissinger theory, which are shown in Fig. 13, resulted in much better agreement with the Kirchheim criterion with desorption energies $E_{D,i}$ of 33.9 kJ/mol and 47.3 kJ/mol for trap 1 and 2, respectively. However, the desorption energy of the second trap is still underestimated. Also, using the asymmetrical peak for the second trap resulted in very similar values as using the improved Gaussian fitting, i.e. 33.8 kJ/mol and 46.7 kJ/mol. Hence, no additional figures with the asymmetrical peak deconvolution were added to the present work.

Finally, the simulated TDS spectra considering three types of trapping sites with binding energies $E_{B,i}$ of 30 kJ/mol, 50 kJ/mol and 70 kJ/mol were evaluated according the Kissinger theory. Similar to the previously simulated TDS spectra with two overlapping peaks, complications arise regarding the

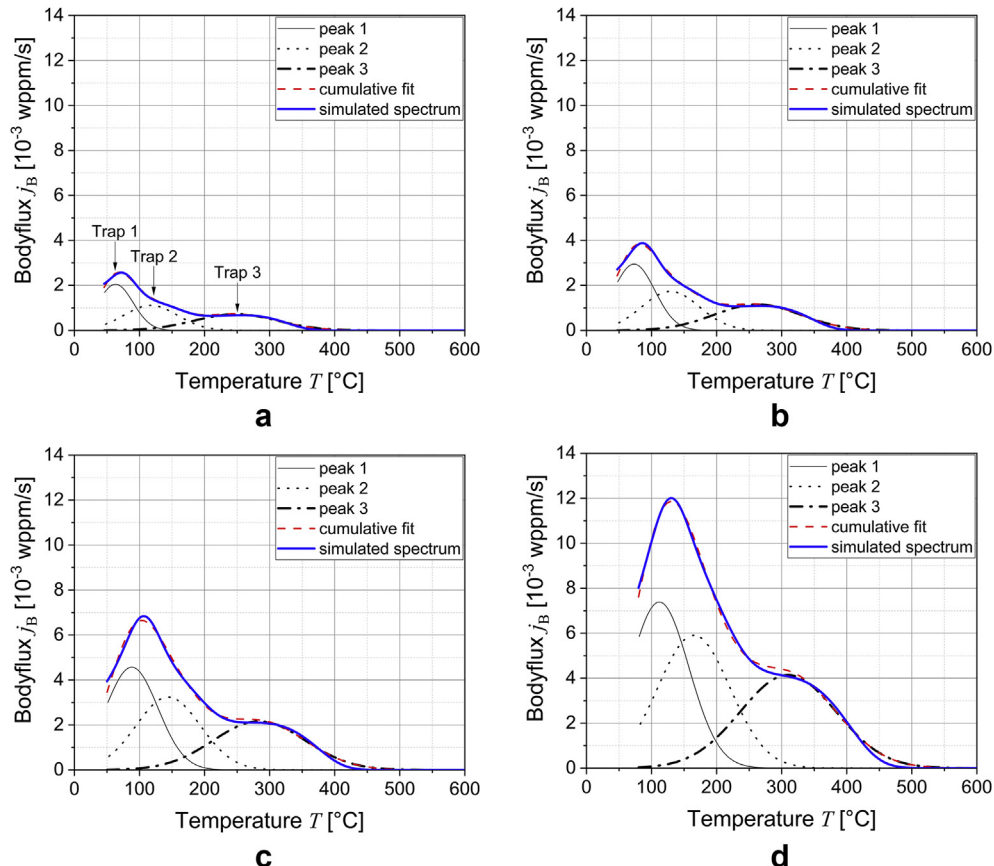


Fig. 16 – Simulated TDS spectra considering three types of trapping sites with binding energies $E_{B,i}$ of 30 kJ/mol, 50 kJ/mol and 70 kJ/mol “Improved” peak deconvolution procedure using Gaussian curves for heating rates θ of a) 0.3 °C/s, b) 0.5 °C/s, c) 1 °C/s and d) 2 °C/s.

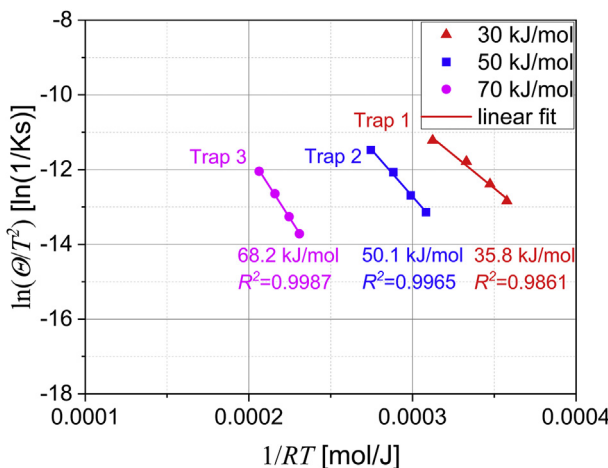


Fig. 17 – Choo-Lee plot of the simulated TDS spectra considering three types of trapping sites with binding energies $E_{B,i}$ of 30 kJ/mol, 50 kJ/mol and 70 kJ/mol. The temperatures of the peak maxima were evaluated by applying the “improved” peak deconvolution procedure using Gaussian curves.

Gaussian peak fitting, as shown in Fig. 14. Simple fitting in combination with the Kissinger equation does not lead to a correct value for the desorption energies $E_{D,i}$, i.e. of 27.2 kJ/mol, 28.1 kJ/mol and 53.4 kJ/mol were obtained for trap 1, trap 2 and trap 3, respectively. However, still very good R^2 -values were obtained for linear fits in the Choo-Lee plot shown Fig. 15. This again confirms that obtaining a good R^2 -values does not guarantee a trustworthy analysis of the TDS spectrum. The desorption energies $E_{D,i}$ evaluated for trap 1 and trap 2 are too close to justify two separate peaks in the TDS spectra from a thermodynamic point of view. A difference of at least the migration energy E_M [60,62,70,71] of approximately 5 kJ/mol is proposed for the desorption energies $E_{D,i}$ to identify two different trapping sites in the microstructures by TDS. Otherwise, the trap densities $N_{T,1}$ and $N_{T,2}$ of two different microstructural defects with the same binding energies $E_{B,1} \equiv E_{B,2}$ are summed up [56] and contribute to the same TDS peak.

Furthermore, the Gaussian peak of trap 2 possesses much smaller area, while the area of the Gaussian peak of trap 1 is rather large. This does not correspond to the parametrization of the bulk diffusion, where the trapped hydrogen concentrations $c_{T,i}$ are of the same order for all trapping site *i*. Therefore, similar restrictions, as described before, were imposed in order to obtain realistic fits, which are shown in Fig. 16. In this case the areas B_2 and B_3 should be approximately equal and about half of B_1 . Again a deviation of 5% was allowed for in the optimization range. According to the Choo-Lee plots shown in Fig. 17, the obtained desorption energies $E_{D,i}$ were 35.8 kJ/mol, 50.1 kJ/mol and 68.2 kJ/mol for trap 1, trap 2 and trap 3, respectively. It can be concluded that in the case of overlapping peaks the first peak of trap 1 can be analysed via the Kissinger theory, but an underestimation of the binding energies $E_{B,i}$ can be found for the other peaks, which appear as shoulders of the first peak in the TDS spectrum.

The presented observations also have important implications on the experimental evaluation of experimental TDS

spectra when using the peak deconvolution procedure according to the Kissinger theory. High R^2 -values of about unity do not necessarily mean that trustworthy desorption energies $E_{D,i}$ have been determined. In order to obtain good fits, appropriate restrictions of the Gaussian peak parameters are mandatory. This requires an in-depth understanding of the microstructure and thus, on the possible types of trapping sites and their trap densities. Without detailed comprehension of the microstructure hydrogen trapping at microstructural defects cannot be evaluated properly.

Summary and conclusions

The objective of the present work was to verify the Kissinger theory with respect to lattice hydrogen diffusion and to the local equilibrium approach according to Oriani's theory. TDS spectra were simulated containing single and multiple hydrogen peaks. The binding energies $E_{B,i}$ were chosen to provide TDS spectra with clearly distinguished peaks as well as overlapping peaks with shoulders. The following conclusions can be drawn:

- Kissinger's theory can be applied to evaluate single or clearly separated peaks in measured TDS spectra.
- The experimentally evaluated desorption energy $E_{D,i}$ according to Kissinger fulfills the Kirchheim criterium $E_{D,i} = E_{B,i} + E_M$, where $E_{B,i}$ is the binding energy of the hydrogen trapping site *i* and E_M is the migration energy of interstitial lattice hydrogen diffusion.
- The evaluation of the TDS spectra with overlapping peaks by using the peak deconvolution procedure is more difficult. The R^2 -values of the linear fit in the Choo-Lee plot were always almost unity and do not necessarily mean that trustworthy desorption energies $E_{D,i}$ according Kissinger have been determined.
- Additional restrictions, e.g. on the areas under the individual peaks, are needed to provide desorption energies fulfilling the Kirchheim criterium. A correct interpretation of complex shaped TDS spectra requires a complete comprehension of the metal microstructure with respect to the types of trapping sites and their trap densities.

Declaration of competing interest

The authors declare that they have no known competing financial interests or personal relationships that could have appeared to influence the work reported in this paper.

Acknowledgements

The authors wish to thank the doctoral and senior post-doctoral fellowship of the Research Foundation Flanders (FWO) via grant 11F6520N and 12Z0420N and the Special Research Fund (BOF), UGent (grants BOF15/BAS/062 and BOF/01J06917) for support.

Appendix

Simulated TDS spectra were fitted by using a superposition of Gaussian peaks as

$$j_B(T) = \sum_{i=1,N} B_i \left(w_i \sqrt{\pi/2} \right)^{-1} \exp \left(-\frac{2(T - T_{m,i})^2}{w_i^2} \right) \quad (19)$$

T is the temperature, $T_{m,i}$ is the temperature of the peak maximum, w_i represents the width of the peak and B_i equals the area under the Gaussian curve for different trapping sites i . All three parameters $T_{m,i}$, w_i and B_i were optimized to minimize the difference between Eq. (19) and the simulated TDS spectra. However, in order to be able to capture more asymmetrical behaviour of the TDS peaks, also a more general peak description was used based on the sum of asymmetric double sigmoidal function, given as

$$j_B(T) = \sum_{i=1,N} C_i \left(1 - \left(1 + \exp \left(-\frac{T - T_{m,i} - v_{1,i}/2}{v_{3,i}} \right) \right)^{-1} \right) \cdot \left(1 + \exp \left(-\frac{T - T_{m,i} + v_{1,i}/2}{v_{2,i}} \right) \right)^{-1} \quad (20)$$

In this case, five parameters need to be optimized for each type of trapping sites i , where $T_{m,i}$ is the temperature of the peak maximum, $v_{1,i}$ is the full width of half maximum (FWHM), $v_{2,i}$ is the variance of the low-temperature side, $v_{3,i}$ the variance of the high-temperature side and C_i is the amplitude.

Nomenclature

A	Constant [–]
B	Area under the Gaussian curve [wppmK/s]
C	Amplitude of the asymmetric peak [wppm/s]
\bar{c}	Total hydrogen content [wppm]
c	Total hydrogen concentration [mol/mm ³]
c_L	Lattice hydrogen concentration [mol/mm ³]
c_T	Total trapped hydrogen concentration [mol/mm ³]
$c_{T,i}$	Trapped hydrogen concentration of trapping site i [mol/mm ³]
D_{chem}	Chemical diffusion coefficient [mm ² /s]
D_{eff}	Effective diffusion coefficient [mm ² /s]
D_L	Tracer diffusion coefficient [mm ² /s]
$D_{L,0}$	Jump frequency [mm ² /s]
θ	Heating rate [°C/s]
$E_{B,i}$	Binding energy of hydrogen trapping site i [kJ/mol]
$E_{D,i}$	Desorption energy of hydrogen trapping site i [kJ/mol]
E_M	Migration energy [kJ/mol]
K_i	Equilibrium constant [–]
i	Trapping sites number ranging from 1 to N [–]
j	Hydrogen diffusion flux [mol/mm ² s]
j_B	Bodyflux [wppm/s]
M_H	Molar mass of hydrogen [g/mol]
N	Total number of hydrogen trapping sites [–]
N_L	Density of interstitial lattice sites [mol/mm ³]
N_T	Total trap density [mol/mm ³]

$N_{T,i}$	Trap density of trapping site i [mol/mm ³]
n	Constant exponent [–]
R	Universal gas constant [mJ/molK]
ϱ	Density of the sample [g/mm ³]
s	Sample thickness [mm]
T	Temperature [K]
T_m	Temperature of the TDS peak maximum [K]
t	Time [s]
$v_{1,i}$	Full width of half maximum of the asymmetric peak (FWHM) [K]
$v_{2,i}$	Variance of the low-temperature side of the asymmetric peak [K]
$v_{3,i}$	Variance of the high-temperature side of the asymmetric peak [K]
Y	Intersection with the y-axis in the Choo-Lee plot [Ks ⁻¹]
y	Mean site fraction of hydrogen in the microstructure [–]
y_L	Site fraction of lattice hydrogen [–]
$y_{T,i}$	Site fraction of trapped hydrogen at trapping site i [–]
w	Width of the Gaussian curve [K]

REFERENCES

- [1] Raabe D, Sun B, Kwiatkowski Da Silva A, Gault B, Yen HW, Sedighiani K, Thoudden Sukumar P, Souza Filho IR, Katnagallu S, Jägle E, Kürnsteiner P, Kusampudi N, Stephenson L, Herbig M, Liebscher CH, Springer H, Zaefererer S, Shah V, Wong SL, Baron C, Diehl M, Roters F, Ponge D. Current challenges and opportunities in microstructure-related properties of advanced high-strength steels. Metall Mater Trans A Phys Metall Mater Sci 2020;51:5517–86. <https://doi.org/10.1007/s11661-020-05947-2>.
- [2] Nagumo M. Fundamentals of hydrogen embrittlement. Singapore: Springer Singapore; 2016. <https://doi.org/10.1007/978-981-10-0161-1>.
- [3] Drexler A, Ecker W, Winzer N, Mraczek K, Kokotin V, Manke G, Bergmann C. A step towards numerical evaluation of the local hydrogen susceptibility of punched and cold-formed advanced high strength steel (AHSS) sheets. In: Duprez L, editor. SteelyHydrogen, oca; 2018. A02. <http://steelyhydrogen2018proc.be/articles/pdf/2>.
- [4] Drexler A, Bergmann C, Manke G, Kokotin V, Mraczek K, Pohl M, Ecker W. On the local evaluation of the hydrogen susceptibility of cold-formed and heat treated advanced high strength steel (AHSS) sheets. Mater Sci Eng 2021;800:140276. <https://doi.org/10.1016/j.msea.2020.140276>.
- [5] Massone A, Manhard A, Drexler A, Posch C, Ecker W, Maier-Kiener V, Kiener D. Addressing H-material interaction in fast diffusion materials—a feasibility study on a complex phase steel. Materials 2020;13:4677. <https://doi.org/10.3390/ma13204677>.
- [6] Massone A, Manhard A, Jacob W, Drexler A, Ecker W, Hohenwarter A, Wurster S, Kiener D. An SEM compatible plasma cell for in situ studies of hydrogen-material interaction. Rev Sci Instrum 2020;91:043705. <https://doi.org/10.1063/1.5142043>.
- [7] Siegl W, Ecker W, Klarner J, Kloesch G, Mori G, Drexler A, Winter G, Schnideritsch H. Hydrogen trapping in heat treated and deformed Armco iron. In: Nace - Int. Corros. Conf. Ser.; 2019. p. 1–12.
- [8] Drexler A, Siegl W, Ecker W, Tkadletz M, Klösch G, Schnideritsch H, Mori G, Svoboda J, Fischer FD. Cycled hydrogen permeation through Armco iron – a joint

- experimental and modeling approach. *Corrosion Sci* 2020;176:109017. <https://doi.org/10.1016/j.corsci.2020.109017>.
- [9] Kholtochina AS, Pippan R, Romaner L, Scheiber D, Ecker W, Razumovskiy VI. Hydrogen trapping in bcc iron. *Materials* 2020;13:2288. <https://doi.org/10.3390/ma13102288>.
- [10] He S, Popov MN, Ecker W, Pippan R, Razumovskiy VI. A theoretical insight into hydrogen clustering at defects in Ni. *Phil Mag Lett* 2021;101:68–78. <https://doi.org/10.1080/09500839.2020.1851054>.
- [11] Vandewalle L, Konstantinović MJ, Depover T, Verbeken K. The potential of the internal friction technique to evaluate the role of vacancies and dislocations in the hydrogen embrittlement of steels. 2021. p. 1–15. <https://doi.org/10.1002/srin.202100037>. 2100037.
- [12] Drexler A, Bergmann C, Manke G, Kokotin V, Mraczek K, Leitner S, Pohl M, Ecker W. Local hydrogen accumulation after cold forming and heat treatment in punched advanced high strength steel sheets. *J Alloys Compd* 2021;856:158226. <https://doi.org/10.1016/j.jallcom.2020.158226>.
- [13] Asahi H, Hirakami D, Yamasaki S. Hydrogen trapping behavior in vanadium-added steel. *ISIJ Int* 2003;43:527–33. <https://doi.org/10.2355/isijinternational.43.527>.
- [14] Saito K, Takai K. Hydrogen desorption behavior trapped in various microstructures of high-strength steels using thermal desorption analysis. *Metall. Mater. Trans. A Phys. Metall. Mater. Sci.* 2021;52:531–43. <https://doi.org/10.1007/s11661-020-06096-2>.
- [15] Takai K, Shoda H, Suzuki H, Nagumo M. Lattice defects dominating hydrogen-related failure of metals. *Acta Mater* 2008;56:5158–67. <https://doi.org/10.1016/j.actamat.2008.06.031>.
- [16] Svoboda J, Mori G, Prethaler A, Fischer FD. Determination of trapping parameters and the chemical diffusion coefficient from hydrogen permeation experiments. *Corrosion Sci* 2014;82:93–100. <https://doi.org/10.1016/j.corsci.2014.01.002>.
- [17] Fischer FD, Mori G, Svoboda J. Modelling the influence of trapping on hydrogen permeation in metals. *Corrosion Sci* 2013;76:382–9. <https://doi.org/10.1016/j.corsci.2013.07.010>.
- [18] Depover T, Hertelé S, Verbeken K. The effect of hydrostatic stress on the hydrogen induced mechanical degradation of dual phase steel: a combined experimental and numerical approach. *Eng Fract Mech* 2019;221:106704. <https://doi.org/10.1016/j.engfracmech.2019.106704>.
- [19] Bhadeshia HKDH. Prevention of hydrogen embrittlement in steels. *ISIJ Int* 2016;56:24–36.
- [20] Pressouyre GM. A classification of hydrogen traps in steel. *Metall. Trans. A* 1979;10:1571–3. <https://doi.org/10.1007/BF02812023>.
- [21] Depover T, Pérez Escobar D, Wallaert E, Zermout Z, Verbeken K. Effect of hydrogen charging on the mechanical properties of advanced high strength steels. *Int J Hydrogen Energy* 2014;39:4647–56. <https://doi.org/10.1016/j.ijhydene.2013.12.190>.
- [22] Rhode M, Wetzel A, Ozcan O, Nietzke J, Richter T, Schroepfer D. Hydrogen diffusion and local Volta potential in high- and medium-entropy alloys. *IOP Conf Ser Mater Sci Eng* 2020;882. <https://doi.org/10.1088/1757-899X/882/1/012015>.
- [23] Pérez Escobar D, Depover T, Duprez L, Verbeken K, Verhaege M. Combined thermal desorption spectroscopy, differential scanning calorimetry, scanning electron microscopy and X-ray diffraction study of hydrogen trapping in cold deformed TRIP steel. *Acta Mater* 2012;60:2593–605. <https://doi.org/10.1016/j.actamat.2012.01.026>.
- [24] Wallaert E, Depover T, Arafat M, Verbeken K. Thermal desorption spectroscopy evaluation of the hydrogen-trapping capacity of NbC and NbN precipitates. *Metall Mater Trans* 2014;45:2412–20. <https://doi.org/10.1007/s11661-013-2181-1>.
- [25] Pérez Escobar D, Depover T, Wallaert E, Duprez L, Verhaege M, Verbeken K. Thermal desorption spectroscopy study of the interaction between hydrogen and different microstructural constituents in lab cast Fe-C alloys. *Corrosion Sci* 2012;65:199–208. <https://doi.org/10.1016/j.corsci.2012.08.017>.
- [26] Depover T, Verbeken K. The effect of TiC on the hydrogen induced ductility loss and trapping behavior of Fe-C-Ti alloys. *Corrosion Sci* 2016;112:308–26. <https://doi.org/10.1016/j.corsci.2016.07.013>.
- [27] Laureys A, Claeys L, De Seranno T, Depover T, Van den Eeckhout E, Petrov R, Verbeken K. The role of titanium and vanadium based precipitates on hydrogen induced degradation of ferritic materials. *Mater Char* 2018;144:22–34. <https://doi.org/10.1016/j.matchar.2018.06.030>.
- [28] Drexler A, Depover T, Verbeken K, Ecker W. Model-based interpretation of thermal desorption spectra of Fe-C-Ti alloys. *J Alloys Compd* 2019;789:647–57. <https://doi.org/10.1016/j.jallcom.2019.03.102>.
- [29] Drexler A, Depover T, Leitner S, Verbeken K, Ecker W. Microstructural based hydrogen diffusion and trapping models applied to Fe–C X alloys. *J Alloys Compd* 2020;826:154057. <https://doi.org/10.1016/j.jallcom.2020.154057>.
- [30] Depover T, Verbeken K. Evaluation of the effect of V4C3 precipitates on the hydrogen induced mechanical degradation in Fe-C-V alloys. *Mater Sci Eng* 2016;675:299–313. <https://doi.org/10.1016/j.msea.2016.08.053>.
- [31] Kissinger HE. Reaction kinetics in differential thermal analysis. *Anal Chem* 1957;29:1702–6. <https://doi.org/10.1021/ac60131a045>.
- [32] Lee JY, Choo WY. Thermal analysis of trapped hydrogen in pure iron. *Metall. Trans. A* 1982;13A:135–40.
- [33] Kirchheim R. Changing the interfacial composition of carbide precipitates in metals and its effect on hydrogen trapping. *Scripta Mater* 2019;160:62–5. <https://doi.org/10.1016/j.scriptamat.2018.09.043>.
- [34] Turk A, Joshi GR, Gintalas M, Callisti M, Rivera-Díaz-del-Castillo PEJ, Galindo-Nava EI. Quantification of hydrogen trapping in multiphase steels: Part I – point traps in martensite. *Acta Mater* 2020;194:118–33. <https://doi.org/10.1016/j.actamat.2020.05.007>.
- [35] Turk A, Pu SD, Bombač D, Rivera-Díaz-del-Castillo PEJ, Galindo-Nava EI. Quantification of hydrogen trapping in multiphase steels: Part II – effect of austenite morphology. *Acta Mater* 2020;197:253–68. <https://doi.org/10.1016/j.actamat.2020.07.039>.
- [36] Turk A, San Martín D, Rivera-Díaz-del-Castillo PEJ, Galindo-Nava EI. Correlation between vanadium carbide size and hydrogen trapping in ferritic steel. *Scripta Mater* 2018;152:112–6. <https://doi.org/10.1016/j.scriptamat.2018.04.013>.
- [37] Polianskiy VA, Belyaev AK, Chevrychkina AA, Varshavchik EA, Yakovlev YUA. Impact of skin effect of hydrogen charging on the Choo-Lee plot for cylindrical samples. *Int J Hydrogen Energy* 2021;46(9):6979–91. <https://doi.org/10.1016/j.ijhydene.2020.11.192>.
- [38] Oriani RA. The diffusion and trapping of hydrogen in steel. *Acta Metall* 1970;18:147–57. [https://doi.org/10.1016/0001-6160\(70\)90078-7](https://doi.org/10.1016/0001-6160(70)90078-7).
- [39] Zügner D, Zamberger S, Yigit N, Rupprechter G, Kozeschnik E. Thermal desorption spectra of H in an Fe–C–Nb alloy evaluated by diffusion simulation. *Steel Res. Int.* 2000;240 2020:1–9. <https://doi.org/10.1002/srin.202000240>.
- [40] Toribio J, Kharin V. A generalised model of hydrogen diffusion in metals with multiple trap types. *Philos Mag* 2015;95:3429–51. <https://doi.org/10.1080/14786435.2015.1079660>.

- [41] Grabke HJ. Surface and grain boundary segregation on and in iron. *Steel Res* 1986;57:178–85. <https://doi.org/10.1002/srin.198600750>.
- [42] Kirchheim R. Bulk diffusion-controlled thermal desorption spectroscopy with examples for hydrogen in iron. *Mater. Trans. A Phys. Metall. Mater. Sci.* 2016;47:672–96. <https://doi.org/10.1007/s11661-015-3236-2>.
- [43] Drexler A, Domitner J, Sommitsch C. Modeling of hydrogen diffusion in slow strain rate (SSR) testing of notched samples. In: VA P, AK B, editors. *Adv. Hydrog. Embrittlement study.* 143rd ed. Springer; 2021. p. 87–111. https://doi.org/10.1007/978-3-030-66948-5_6.
- [44] Song EJ, Suh DW, Bhadeshia HKDH. Theory for hydrogen desorption in ferritic steel. *Comput Mater Sci* 2013;79:36–44. <https://doi.org/10.1016/j.commatsci.2013.06.008>.
- [45] Drexler A, He S, Pippan R, Romaner L, Razumovskiy VI, Ecker W. Hydrogen segregation near a crack tip in nickel. *Scripta Mater* 2021;194:113697. <https://doi.org/10.1016/j.scriptamat.2020.113697>.
- [46] Drexler A, He S, Razumovskiy V, Romaner L, Ecker W, Pippan R. Verification of the generalised chemical potential for stress-driven hydrogen diffusion in nickel. *Phil Mag Lett* 2020;100:513–23. <https://doi.org/10.1080/09500839.2020.1808253>.
- [47] Fischer FD, Svoboda J, Kozeschnik E. Interstitial diffusion in systems with multiple sorts of traps. *Model Simulat Mater Sci Eng* 2013;21:025008. <https://doi.org/10.1088/0965-0393/21/2/025008>.
- [48] Toribio J, Lancha AM, Elices M. Macroscopic variables governing the microscopic fracture of pearlitic steels. *Mater Sci Eng* 1991;145:167–77. [https://doi.org/10.1016/0921-5093\(91\)90246-J](https://doi.org/10.1016/0921-5093(91)90246-J).
- [49] Raina A, Deshpande VS, Fleck NA. Analysis of thermal desorption of hydrogen in metallic alloys. *Acta Mater* 2018;144:777–85. <https://doi.org/10.1016/j.actamat.2017.11.011>.
- [50] Soustelle M. An introduction to chemical kinetics. 2011. <https://doi.org/10.1002/9781118604243>.
- [51] Enomoto M, Hirakami D, Tarui T. Modeling thermal desorption analysis of hydrogen in steel. *ISIJ Int* 2006;46:1381–7. <https://doi.org/10.2355/isijinternational.46.1381>.
- [52] Depover T, Verbeken K. Hydrogen trapping and hydrogen induced mechanical degradation in lab cast Fe-C-Cr alloys. *Mater Sci Eng* 2016;669:134–49. <https://doi.org/10.1016/j.msea.2016.05.018>.
- [53] Rhode M, Mente T, Steppan E, Steger J, Kannengiesser T. Hydrogen trapping in T24 Cr-Mo-V steel weld joints—microstructure effect vs. experimental influence on activation energy for diffusion. *Weld World* 2018;62:277–87. <https://doi.org/10.1007/s40194-017-0546-6>.
- [54] Drexler A, Gänser HP, Ecker W, Oberwinkler B, Fischersworing-Bunk A. Computationally efficient models for the forced air cooling of turbine disks. In: *Therm. Process model. - Proc. From 5th Int. Conf. Therm. Process model. Comput. Simulation, ICTPMCS. vol. 2014*; 2014. p. 223–31.
- [55] Polyanskiy VA, Belyaev AK, Alekseeva EL, Polyanskiy AM, Tretyakov DA, Yakovlev YA. Phenomenon of skin effect in metals due to hydrogen absorption. *Continuum Mech Therm* 2019;31:1961–75. <https://doi.org/10.1007/s00161-019-00839-2>.
- [56] Svoboda J, Fischer FD. Modelling for hydrogen diffusion in metals with traps revisited. *Acta Mater* 2012;60:1211–20. <https://doi.org/10.1016/j.actamat.2011.11.025>.
- [57] Jiang DE, Carter EA. Diffusion of interstitial hydrogen into and through bcc Fe from first principles. *Phys Rev B* 2004;70:064102. <https://doi.org/10.1103/PhysRevB.70.064102>.
- [58] Paxton AT, Elsässer C. Electronic structure and total energy of interstitial hydrogen in iron: tight-binding models. *Phys Rev B Condens Matter* 2010;82:235125. <https://doi.org/10.1103/PhysRevB.82.235125>.
- [59] Wipf H. Solubility and diffusion of hydrogen in pure metals and alloys. *Phys Scripta* 2001;43:138–48. <https://doi.org/10.1238/Physica.Topical.094a00043>.
- [60] Grabke HJ, Riecke E. Absorption and diffusion of hydrogen in steels. *Mater. Tehnol.* 2000;34:331–432.
- [61] Hagi H, Hayashi Y, Ohtani N. Diffusion coefficient of hydrogen in pure iron between 230 and 300 K. *Trans. Japan Inst. Met.* 1979;20:349–57. <https://doi.org/10.2320/matertrans1960.20.349>.
- [62] Kiuchi K, McLellan RB. The solubility and diffusivity of hydrogen in well-annealed and deformed iron. *Acta Metall* 1983;31:961–84. [https://doi.org/10.1016/0001-6160\(83\)90192-X](https://doi.org/10.1016/0001-6160(83)90192-X).
- [63] Drexler A, Helic B, Silvayeh Z. The role of hydrogen diffusion, trapping and desorption in dual phase steels. *Submitt. to J. Mater. Sci.* 2021;1–30.
- [64] Depover T, Verbeken K. The detrimental effect of hydrogen at dislocations on the hydrogen embrittlement susceptibility of Fe-C-X alloys: an experimental proof of the HELP mechanism. *Int J Hydrogen Energy* 2018;43:3050–61. <https://doi.org/10.1016/j.ijhydene.2017.12.109>.
- [65] Depover T, Hajilou T, Wan D, Wang D, Barnoush A, Verbeken K. Assessment of the potential of hydrogen plasma charging as compared to conventional electrochemical hydrogen charging on dual phase steel. *Mater Sci Eng* 2019;754:613–21. <https://doi.org/10.1016/j.msea.2019.03.097>.
- [66] Pressouyre GM, Bernstein IM. A quantitative analysis of hydrogen trapping. *Mater. Trans. A.* 1978;9:1571–80. <https://doi.org/10.1007/BF02661939>.
- [67] Di Stefano D, Nazarov R, Hickel T, Neugebauer J, Mrovec M, Elsässer C. First-principles investigation of hydrogen interaction with TiC precipitates in α -Fe. *Phys Rev B* 2016;93:184108. <https://doi.org/10.1103/PhysRevB.93.184108>.
- [68] Bergmann C. *Hydrogen embrittlement resistance of advanced high strength steel grades in automotive applications*. Ruhr-Universität Bochum; 2020.
- [69] Paxton T, Frs APS, Finnis MW. The challenges of hydrogen and metals. *Philos. Trans. R. Soc. A Math. Phys. Eng. Sci.* 2017;375. <https://doi.org/10.1098/rsta.2017.0198>.
- [70] Nelson HG, Stein JE. Gas-phase hydrogen permeation through alpha iron, 4130 steel, and 304 stainless steel from less than 100 °C to near 600 °C, Washington, D.C.. 1973. <http://hdl.handle.net/2060/19730012715>.
- [71] Hagi H. Diffusion coefficient of hydrogen in iron without trapping by dislocations and impurities. *Mater Trans JIM* 1994;35:112–7. <https://doi.org/10.2320/matertrans1989.35.112>.